Featured in Physics

Single-Photon Synchronization with a Room-Temperature Atomic Quantum Memory

Omri Davidson,* Ohad Yogev, Eilon Poem, and Ofer Firstenberg
Department of Physics of Complex Systems, Weizmann Institute of Science, Rehovot 7610001, Israel

(Received 21 February 2023; accepted 31 May 2023; published 18 July 2023)

Efficient synchronization of single photons that are compatible with narrow band atomic transitions is an outstanding challenge, which could prove essential for photonic quantum information processing. Here we report on the synchronization of independently generated single photons using a room-temperature atomic quantum memory. The photon source and the memory are interconnected by fibers and employ the same ladder-level atomic scheme. We store and retrieve the heralded single photons with end-to-end efficiency of $\eta_{\mathrm{e2e}} = 25\%$ and final antibunching of $g_h^{(2)} = 0.023$. Our synchronization process results in an over tenfold increase in the photon-pair coincidence rate, reaching a rate of more than 1000 detected synchronized photon pairs per second. The indistinguishability of the synchronized photons is verified by a Hong-Ou-Mandel interference measurement.

DOI: 10.1103/PhysRevLett.131.033601

Multiphoton states are an important resource for photonic quantum information processing, with potential applications in quantum computation, communication, and metrology [1–4]. It is beneficial that these photons interact coherently with atomic ensembles, to enable the implementation of deterministic two-photon gates [5] and quantum repeaters for long-distance communication [6]. Efficient, well-established, room-temperature platforms for generating such photons are based on parametric processes such as spontaneous parametric down-conversion (SPDC) and four-wave mixing (FWM) [7]. These processes give rise to stochastic emission of photon pairs and are therefore utilized as heralded single-photon sources [8–11]. However, they are probabilistic, rendering the construction of larger multiphoton states exponentially slow [12]. At present, the demonstrated rate for generating a 12-photon entangled state from six stochastic emission events is one per hour [13].

The exponential scaling of the rate with the number of photons N can be mitigated by using quantum memories to synchronize the probabilistically generated photons [12]. Particularly, the quantum memory can support a time-multiplexing scheme, generating a string of quasideterministic photons at predetermined clock cycles [14–16]. Alternatively, N stochastic photon sources with $N-1$ memories can be used to generate a synchronous N-photon state [12,17]. Most works focus on $N=2$, and we do so as well.

For $N=2$, we identify several key metrics. The first is the rate enhancement factor $\zeta = R_{\mathrm{sync}}/R_{\mathrm{stoc}}$, which is the accomplishment of the synchronization, the ratio between the detection rate of photon pairs after the synchronization R_{sync} compared to the stochastic (accidental) pair detection rate before synchronization R_{stoc}. The second is R_{sync}, which should be high for practical applications. A third metric is the antibunching of the synchronized photons $g_h^{(2)}$, which is the normalized autocorrelation of the retrieved signal field conditioned on heralding. Ideally, $g_h^{(2)} = 0$, and any undesired multiphoton component, e.g., due to noise, increases $g_h^{(2)}$.

There are two types of memories: those containing an internal source [18–20] and input-output memories accepting photons from outside [21–23]. The natural advantage of input-output memories is that they can be used to synchronize and delay photons that have already undergone some processing, including photons that are part of larger entangled states. Photon synchronization has been demonstrated with cold [24–27] and hot [28] atomic ensembles, employing internal-source memories [24–26,28] and input-output memories [27]. However, all these demonstrations suffer from a low photon-pair synchronization rate ($R_{\mathrm{sync}} < 1$ counts/s) and moderate photon antibunching ($g_h^{(2)} > 0.15$). For a comparison of different photon synchronization experiments, see Table S1 in the Supplemental Material [29].

A successful competing approach to atomic memories uses all-optical setups, namely, cavities [34,35] and storage loops [14–17,36–38]. Cavity systems have achieved good performance with narrow band photons, $\zeta = 25$ and $R_{\mathrm{sync}} = 90$ counts/s [35], but these are internal-source systems. Storage loops, which are input-output systems, have reached $\zeta = 30$ and $R_{\mathrm{sync}} = 450$ counts/s with broadband SPDC photons [16,17,37] but inferior performance with narrow band photons [36]. Notably, interfacing atomic ensembles with broadband photons, such as those generated from SPDC without a cavity, remains an outstanding challenge.

Here we demonstrate for the first time single-photon synchronization using an input-output memory that combines substantial rate enhancement $10 \leq \zeta \leq 30$, high pair detection rates $R_{\mathrm{sync}} \leq 1200$ counts/s, low-noise operation with $g_h^{(2)} = 0.023$, and compatibility with atomic ensembles. We achieve these at room temperature by employing the ladder orbital scheme $|5S_{1/2}\rangle \to |5P_{3/2}\rangle \to |5D_{5/2}\rangle$ in rubidium vapor for the photon source [39–41] *and* for the quantum memory [42,43]. This scheme has three main benefits. First, the all-orbital fast ladder memory (FLAME) provides high-bandwidth operation, low noise, and high end-to-end memory efficiency [42–44], which are key for high-rate single-photon synchronization. Second, the small wavelength mismatch within the two-photon transition enables a nearly Doppler-free operation and thus a long coherence time between the ground and doubly excited state. This provides a memory lifetime of over 100 ns [43] and single-photon generation with high rate and low noise [39–41]. Third, by employing the same level scheme for the photon source and quantum memory, the generated photons are inherently compatible with the memory, enabling an end-to-end memory efficiency of $\eta_{\mathrm{e2e}} = 25\%$. This also maintains the indistinguishability of the synchronized photons, as quantified by the Hong-Ou-Mandel (HOM) interference visibility $V_{\mathrm{sync}} = 76\%$.

Synchronization scheme.—The synchronization experiment comprises a spatially multiplexed single-photon source, a quantum memory, and electronic triggering of the memory operation, as shown schematically in Fig. 1. The photon source is based on FWM in rubidium vapor with two continuous-wave pump fields [40,41]. The pump fields, at wavelengths of 780 and 776 nm, counterpropagate through an isotopically purified ^{87}Rb vapor cell and excite the $|5S_{1/2}, F = 2\rangle \to |5P_{3/2}, F = 3\rangle$ and $|5P_{3/2}, F = 3\rangle \to |5D_{5/2}, F = 4\rangle$ transitions, respectively. The detection of a spontaneously emitted idler photon heralds the generation of a collective state comprising a single $|5P_{3/2}\rangle$ excitation that is shared among all atoms, and the signal photon emission to the ground state is thus collectively enhanced into the phase-matched direction [45]. We utilize the cylindrical symmetry of the phase-matching condition to set collection channels on both sides of the optical axis, effectively realizing two sources in the same vapor cell. We denote the generated photons in channel j as idler j and signal j ($j = 1, 2$). Additional details on the photon source are given in the Supplemental Material [29] and in Refs. [40,41].

The quantum memory is based on the FLAME scheme in ^{87}Rb vapor [42,43]. Initially, the atoms in the memory cell are optically pumped to the maximal spin state. An input signal-1 photon, which couples to the $|5S_{1/2}, F = 2, m_F = 2\rangle \to |5P_{3/2}, F = 3, m_F = 3\rangle$ transition, is stored on the doubly excited state $|5D_{5/2}, F = 4, m_F = 4\rangle$ by sending the first (storage) control pulse. At a controllable time later,

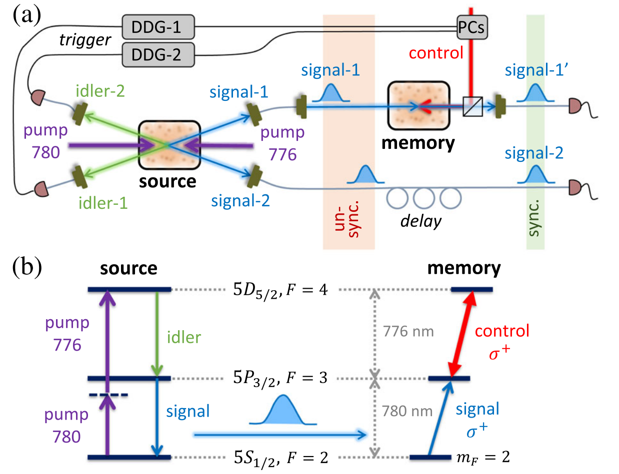

FIG. 1. Photon synchronization scheme. (a) Sketch of the experimental setup. Two pump fields continuously excite the atoms in the source module, which then emit signal and idler photons in two phase-matched directions via four-wave mixing. Signal 1 photon in the first collection channel goes to the memory module, while the detection of idler 1 triggers the control storage pulse in the memory [generated by PCs]. Signal 2 in the second collection channel goes into a fiber delay line, while the detection of idler 2 triggers the control retrieval pulse, which releases signal 1′ from the memory synchronously with signal 2. (b) The photon source and memory both employ the same ladder-type level system of ^{87}Rb, which is nearly Doppler-free and enables high storage efficiency and fidelity.

a second (retrieval) control pulse releases the signal-1′ photon from the memory (1′ marks postmemory). We use an auxiliary dressing field (not shown in Fig. 1) that weakly couples the storage state $|5D_{5/2}\rangle$ to a high-lying orbital in order to counteract the residual Doppler broadening of the two-photon transition [46] and prolong the memory lifetime [43]. The overall transmission of the memory module from the input fiber to the output fiber is $T = 71 \pm 2\%$. Further details on the memory are given in the Supplemental Material [29] and in Ref. [43].

The detection of idler photons triggers digital delay generators (DDGs) that set off the control pulses for the memory via free-space Pockels cells (PCs). DDG 1, triggered by idler 1, sends a control pulse that stores the heralded signal 1 in the memory. Subsequently, DDG 2, triggered by idler 2, sends a second control pulse that retrieves signal 1′. This protocol synchronizes signal 1′ and signal 2. We find that the memory efficiency is optimal when the control field is on resonance, indicating that signal 1 is emitted from the source on resonance, as expected [41]. As our PCs' maximal average repetition rate is limited to 3×10^5 operations/s, we devise a logical scheme that operates them only if idler 1 and idler 2 are both detected within a 100-ns time window, set by the memory lifetime. Details on the electronic triggering, timing sequence, and fiber routing are given in the Supplemental Material [29].

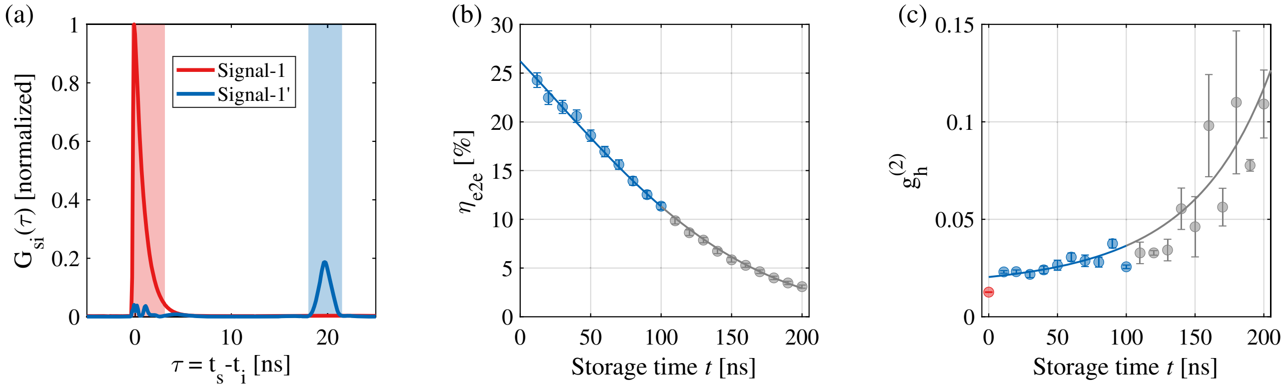

FIG. 2. Storage of heralded single photons. (a) Raw histogram counts (signal-idler cross-correlation) without storage (signal 1, red) and after storage and retrieval in the memory (signal 1′, blue). Here $\tau = t_s - t_i$ is the time difference between detections of the signal and idler photons. The shaded areas indicate the 3.5-ns-long integration window used throughout the paper. (b) End-to-end memory efficiency versus storage time of heralded single photons. Circles are the measured data, and the line is a fit to a model of exponential and Gaussian decays. The error bars comprise the standard error of repeated measurements and the uncertainty on the detection efficiencies of signal 1 and signal 1′ (see Supplemental Material [29]). (c) The normalized autocorrelation of signal 1′ conditioned on the detection of idler 1, $g_h^{(2)}$, indicating the multiphoton component in the retrieved field. The $g_h^{(2)}$ of unstored photons (signal 1) is shown in red for reference. The line is a fit to a model comprising the finite memory efficiency and assuming that noise photons originate only from the source. (b),(c) Blue indicates the range of storage times $t \leq 100$ ns used in the synchronization experiment.

Storage and retrieval of heralded single photons.—We begin by characterizing the storage and retrieval of signal 1. Figure 2(a) shows the count histogram [signal-idler correlation $G_{si}(\tau)$] for a storage time of $t = 20$ ns. We compare the histogram of signal 1 (i.e., directly after the photon source) to that of signal 1′ (i.e., after storage and retrieval in the memory, including the overall transmission of the memory module). The 3.5-ns-long shaded areas indicate the integration windows used for calculating η_{e2e}, $g_h^{(2)}$, R_{stoc}, R_{sync}, and V_{sync}; This window captures over 95% of the pulse energy.

The memory efficiency η_{e2e} versus the storage time t is shown in Fig. 2(b). Here, we directly measure the end-to-end efficiency by connecting the optical fiber of signal 1 either to the memory input fiber ($98 \pm 1\%$ coupling) or directly to the detector input fiber ($92 \pm 1\%$ coupling). Comparing between the detection rates of signal 1 and signal 1′, after correcting for the different couplings, provides η_{e2e}. Note, particularly, that η_{e2e} includes all fiber/free-space couplings. We measure $\eta_{e2e}(t = 12\text{ ns}) = 24.3 \pm 0.8\%$. By fitting the data to a decoherence model $\eta(t) = \eta(0)e^{-t^2/2\tau_\sigma^2 - t/\tau_\gamma}$ with homogeneous (τ_γ) and inhomogeneous (τ_σ) decoherence times, we extract the zero-time memory efficiency $\eta_{e2e}(0) = 26.2 \pm 0.5\%$. The memory $1/e$ lifetime is $\tau_s = 114 \pm 2$ ns. Here the errors are 1 standard deviation of the fit uncertainty. Given the overall transmission T, the memory internal efficiency, comprising only the mapping of the light to and from the atoms, is $\eta_{int}(0) = 36.9 \pm 1.1\%$.

We verify that the memory preserves the quantum statistics $g_h^{(2)} \ll 1$ of the stored single photons, as shown in Fig. 2(c). For $t = 20$ ns, the multiphoton component of signal 1′ is $g_h^{(2)} = 0.023 \pm 0.001$, which is higher than $g_h^{(2)} = 0.0126 \pm 0.0002$ of signal 1 but still at the few-percent level.

The increase in $g_h^{(2)}$ is due to noise photons originating in either the memory or the source. In our system, the former is negligible: the memory generates only $\nu = (1.7 \pm 0.2) \times 10^{-5}$ noise photons per operation. These photons govern the short-time signal-to-noise ratio $\text{SNR} = \eta_h \eta_{e2e}(0)/\nu = 3100 \pm 400$, where $\eta_h = 20\%$ is the heralding efficiency of the source, and indeed $\text{SNR}^{-1} \ll g_h^{(2)}$. Therefore, we attribute the increase in $g_h^{(2)}$ predominantly to noise photons arriving from the source at the time of retrieval and detected in coincidence with signal 1′. The dominant contribution comes from photons that scatter directly from the continuous, off-resonant, 780-nm pump field, which are transmitted well through the memory module. Further increase of $g_h^{(2)}(t)$ at larger t is explained solely by the decrease of $\eta_{e2e}(t)$. Our model of this mechanism, shown in Fig. 2(c) and detailed in the Supplemental Material [29], agrees well with the data.

Photon synchronization.—We now turn to demonstrate the synchronization of photon pairs using the memory. Figure 3(a) shows temporal profiles of the retrieved signal-1′ photons (signal-1′-idler-2 correlation conditioned on memory operation, $G_{s1'i2}$) in comparison to the profile of signal 2 (signal-2-idler-2 correlation, G_{s2i2}) for varying timing settings. Note that the data do not correspond to a specific memory time t but rather represent an average over $0 < t \leq 100$ ns, stochastically "sampled" by the regular operation of the synchronization protocol. We control the exact relative timing Δt between signal 1′ and signal 2 by

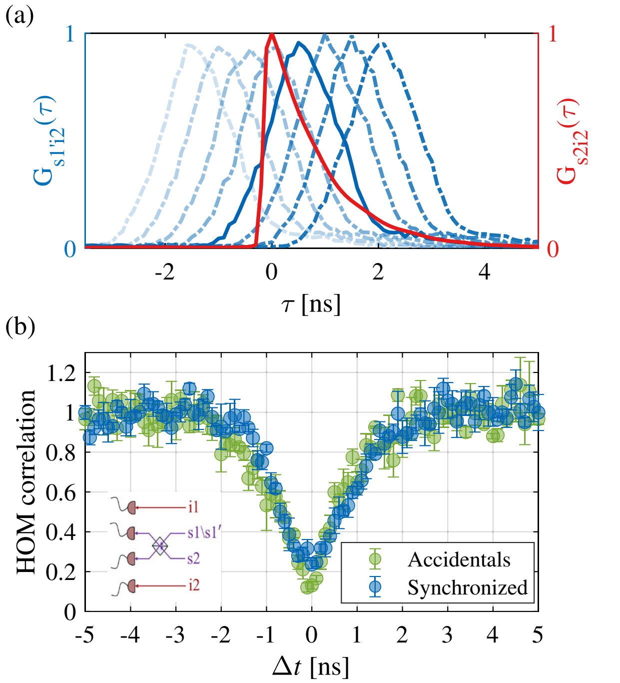

FIG. 3. Photon synchronization. (a) Histograms of signal-2-idler-2 correlation (red) and signal-1′-idler-2 correlation (blue), demonstrating the synchronization of signal 1′ with signal 2. The curves with different shades of blue correspond to different controlled retrieval times of signal 1′ with 500 ps intervals. The solid blue curve corresponds to the synchronized signal 1′. (b) HOM interference between photons originating from the two source channels. Without the memory (signal-1-signal-2, green), Δt is the time difference between idler 1 and idler 2. With the memory and synchronization (signal-1′-signal-2, blue), Δt is controlled by tuning the electronic delay between idler 2 (trigger) and signal 1′ (memory retrieval). The inset shows a schematic of the detection scheme.

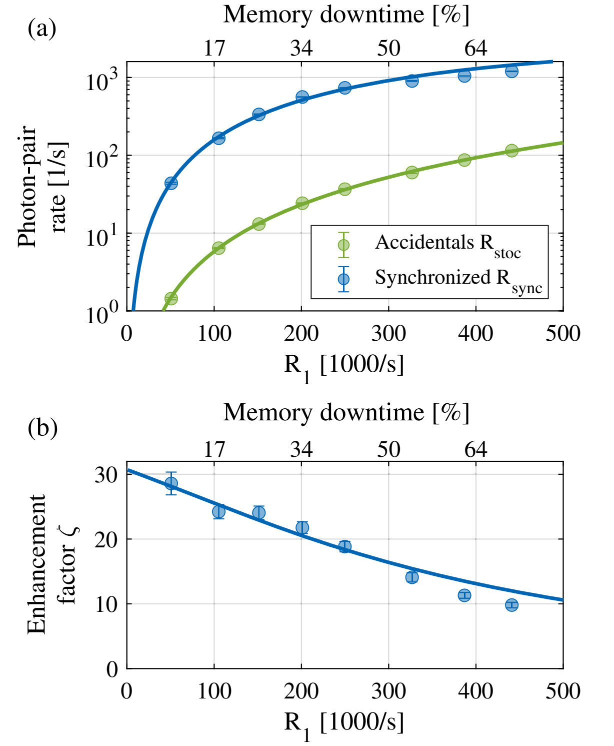

FIG. 4. Rate enhancement by synchronization. (a) Pair coincidence count rate with the memory (R_{sync}, blue) and without the memory (R_{stoc}, green) versus the single-photon count rate R_1. (b) The enhancement factor $\zeta = R_{sync}/R_{stoc}$ of pair coincidence rate. Circles are measured data, and the lines are calculations based on independently measured parameters of the source and memory with no fit parameters. The top horizontal axes show the relative downtime of the memory, during which it cannot handle photons for synchronization due to technical limitations. This downtime quantifies the technical saturation of the system, responsible for the degradation of ζ with R_1.

electronically tuning the trigger delay, which controls the memory retrieval time. Figure 3(a) demonstrates, for arbitrary 500-ps intervals, our capability of on-demand, continuous tuning of the retrieval time.

To optimize the relative timing and to characterize the fidelity of the synchronized photons, we perform HOM interference measurements [47]. These measurements attest to the indistinguishability of the synchronized photon pair. Figure 3(b) shows the HOM correlation of signal 1′ and signal 2 for varying triggering delays. The HOM visibility (the interference contrast), quantifying the indistinguishability, is $V_{sync} = 76 \pm 2\%$. We use the position of the minimum to define $\Delta t = 0$ and to set the optimal delays in the system. For reference, we show in Fig. 3(b) the HOM measurement of accidental pairs without the memory, exhibiting $V_{stoc} = 88 \pm 2\%$. Notably, the acquisition time per data point for synchronized pairs is 100 times shorter than for accidental pairs, illustrating the importance of synchronization for efficiently manipulating multiphoton states.

Finally, we show the merit of synchronization in terms of the enhanced two-photon coincidence rate R_{sync} in Fig. 4(a). We study R_{sync} as a function of the heralded single-photon rate R_1, which we control by tuning the strength of the pumps in the source module. We cover the range $50 < R_1 < 440$ kilocounts/s, for which the accidental coincidence rates are $1.4 < R_{stoc} < 115$ counts/s. Here, we consider an accidental coincidence if idler 1 and idler 2 are detected within ± 300 ps of each other. This time interval is chosen based on the HOM correlation measurement, which exhibits $V_{stoc} \geq 75\%$ within ± 300 ps around the minimum, comparable to V_{sync}. As shown in Fig. 4(a), the coincidence rates after synchronization grow to $44 < R_{sync} < 1200 \pm 10$ counts/s, a substantial enhancement compared to R_{stoc}.

The rate enhancement $\zeta = R_{sync}/R_{stoc}$ is shown in Fig. 4(b). The maximal enhancement $\zeta = 28.6 \pm 1.8$ is obtained at low R_1. As R_1 increases, the system is triggered more often, and each triggering event is followed by ~ 1 μs during which the memory cannot handle additional photons (see the Supplemental Material [29] for details). This leads to technical saturation of the system, which we quantify by the relative memory downtime, shown as top axes in Fig. 4. A second issue occurring at high R_1 is a moderate increase of $g_h^{(2)}$ and a corresponding decrease of V_{sync} (see Supplemental Material [29]), due mainly to the higher $g_h^{(2)}$ directly after the photon source and to the saturation of the memory. Nevertheless, even at the highest rate, we obtain a tenfold increase in the pair coincidence rate and a nonclassical HOM visibility $V_{\mathrm{sync}} > 50\%$.

The rates of accidental and synchronized photon pairs and their dependence on the rate of single photons can be calculated from the parameters of the source, memory, and electronics, all of which we have independently characterized. Our model, based solely on these parameters without fitting (see the Supplemental Material [29] for details), is presented by the solid lines in Fig. 4. The model correctly predicts R_{sync} and R_{stoc} and confirms that the decrease of ζ with R_1 is due only to the memory downtime. We attribute the slight deviation of the model from the data at large R_1 to a degradation of the amplitude of the pulses generated by the PCs at a high triggering rate. This pulse degradation also partially contributes to the increase in $g_h^{(2)}$ and decrease in V_{sync} noted above.

Discussion.—There are several factors limiting the increase of the two-photon coincidence rate. The main ones are the end-to-end efficiency of the memory, the limited operation rate of the PCs, and the heralding efficiency of the photon source. All these factors can be improved.

First, as discussed in Ref. [43], practicable technical improvements of the memory module can increase the internal memory efficiency to 65%. This, in addition to raising the setup transmission by antireflection coating of the optical fiber-to-free-space interfaces, will substantially raise the end-to-end efficiency. Second, the heralding efficiency of the photon source can be increased by using etalon filters to block the direct scattering of photons from the pump fields into the idler modes. Third, the PCs can be replaced by an amplitude electro-optic modulator seeding a tapered amplifier [23]. This will enable both a higher repetition rate and a higher memory efficiency by optimizing the control temporal shape to that of the signal photons [48,49].

Our scheme can also be used to synchronize $N > 2$-photon states by increasing the number of sources and memories. With the current performance, a three (four)-photon state can be generated with a rate greater than 10 (0.1) counts/s, and with the improvements discussed above, a six-photon state can be generated with a rate greater than 0.1 counts/s (see the Supplemental Material [29]). The main limitation for large N-photon states becomes the heralding efficiency of the photon source, which may be enhanced by employing a cavity around the signal and idler modes.

In conclusion, we demonstrate synchronization of single photons with a high rate and low noise using a quantum memory and a photon source, both based on a ladder-level scheme in rubidium vapor. Our synchronized photons are well suited for quantum information protocols requiring efficient interaction with atomic ensembles, such as Rydberg-mediated deterministic two-photon gates.

We acknowledge financial support from the Israel Science Foundation, the U.S.-Israel Binational Science Foundation (BSF) and U.S. National Science Foundation (NSF), the Minerva Foundation with funding from the Federal German Ministry for Education and Research, the estate of Louise Yasgour, and the Laboratory in Memory of Leon and Blacky Broder.

*Corresponding author.
omri.davidson@weizmann.ac.il

[1] Fulvio Flamini, Nicolò Spagnolo, and Fabio Sciarrino, Photonic quantum information processing: A review, Rep. Prog. Phys. **82**, 016001 (2018).

[2] E. Knill, R. Laflamme, and G. J. Milburn, A scheme for efficient quantum computation with linear optics, Nature (London) **409**, 46 (2001).

[3] Koji Azuma, Kiyoshi Tamaki, and Hoi-Kwong Lo, All-photonic quantum repeaters, Nat. Commun. **6**, 6787 (2015).

[4] Jonathan P. Dowling, Quantum optical metrology—the lowdown on high-N00N states, Contemp. Phys. **49**, 125 (2008).

[5] O. Firstenberg, C. S. Adams, and S. Hofferberth, Nonlinear quantum optics mediated by Rydberg interactions, J. Phys. B **49**, 152003 (2016).

[6] L. M. Duan, M. D. Lukin, J. I. Cirac, and P. Zoller, Long-distance quantum communication with atomic ensembles and linear optics, Nature (London) **414**, 413 (2001).

[7] M. D. Eisaman, J. Fan, A. Migdall, and S. V. Polyakov, Invited review article: Single-photon sources and detectors, Rev. Sci. Instrum. **82**, 071101 (2011).

[8] Hanna Le Jeannic, Varun B. Verma, Adrien Cavaillès, Francesco Marsili, Matthew D. Shaw, Kun Huang, Olivier Morin, Sae Woo Nam, and Julien Laurat, High-efficiency WSi superconducting nanowire single-photon detectors for quantum state engineering in the near infrared, Opt. Lett. **41**, 5341 (2016).

[9] Chih-Hsiang Wu, Tsung-Yao Wu, Yung-Chin Yeh, Po-Hui Liu, Chin-Hsuan Chang, Chiao-Kai Liu, Ting Cheng, and Chih-Sung Chuu, Bright single photons for light-matter interaction, Phys. Rev. A **96**, 023811 (2017).

[10] Daniel Llewellyn, Yunhong Ding, Imad I. Faruque, Stefano Paesani, Davide Bacco, Raffaele Santagati, Yan-Jun Qian, Yan Li, Yun-Feng Xiao, Marcus Huber, Mehul Malik, Gary F. Sinclair, Xiaoqi Zhou, Karsten Rottwitt, Jeremy L. O'Brien, John G. Rarity, Qihuang Gong, Leif K. Oxenlowe, Jianwei Wang, and Mark G. Thompson, Chip-to-chip quantum teleportation and multi-photon entanglement in silicon, Nat. Phys. **16**, 148 (2020).

[11] Gurpreet Kaur Gulati, Bharath Srivathsan, Brenda Chng, Alessandro Cerè, Dzmitry Matsukevich, and Christian Kurtsiefer, Generation of an exponentially rising single-photon field from parametric conversion in atoms, Phys. Rev. A **90**, 033819 (2014).
[12] J. Nunn, N. K. Langford, W. S. Kolthammer, T. F. M. Champion, M. R. Sprague, P. S. Michelberger, X.-M. Jin, D. G. England, and I. A. Walmsley, Enhancing Multiphoton Rates with Quantum Memories, Phys. Rev. Lett. **110**, 133601 (2013).
[13] Han-Sen Zhong, Yuan Li, Wei Li, Li-Chao Peng, Zu-En Su, Yi Hu, Yu-Ming He, Xing Ding, Weijun Zhang, Hao Li, Lu Zhang, Zhen Wang, Lixing You, Xi-Lin Wang, Xiao Jiang, Li Li, Yu-Ao Chen, Nai-Le Liu, Chao-Yang Lu, and Jian-Wei Pan, 12-Photon Entanglement and Scalable Scattershot Boson Sampling with Optimal Entangled-Photon Pairs from Parametric Down-Conversion, Phys. Rev. Lett. **121**, 250505 (2018).
[14] T. B. Pittman, B. C. Jacobs, and J. D. Franson, Single photons on pseudodemand from stored parametric down-conversion, Phys. Rev. A **66**, 042303 (2002).
[15] Fumihiro Kaneda, Bradley G. Christensen, Jia Jun Wong, Hee Su Park, Kevin T. McCusker, and Paul G. Kwiat, Time-multiplexed heralded single-photon source, Optica **2**, 1010 (2015).
[16] F. Kaneda and P. G. Kwiat, High-efficiency single-photon generation via large-scale active time multiplexing, Sci. Adv. **5**, eaaw8586 (2019).
[17] Fumihiro Kaneda, Feihu Xu, Joseph Chapman, and Paul G. Kwiat, Quantum-memory-assisted multi-photon generation for efficient quantum information processing, Optica **4**, 1034 (2017).
[18] Shuai Chen, Yu-Ao Chen, Thorsten Strassel, Zhen-Sheng Yuan, Bo Zhao, Jörg Schmiedmayer, and Jian-Wei Pan, Deterministic and Storable Single-Photon Source Based on a Quantum Memory, Phys. Rev. Lett. **97**, 173004 (2006).
[19] Erwan Bimbard, Rajiv Boddeda, Nicolas Vitrant, Andrey Grankin, Valentina Parigi, Jovica Stanojevic, Alexei Ourjoumtsev, and Philippe Grangier, Homodyne Tomography of a Single Photon Retrieved on Demand from a Cavity-Enhanced Cold Atom Memory, Phys. Rev. Lett. **112**, 033601 (2014).
[20] Karsten B. Dideriksen, Rebecca Schmieg, Michael Zugenmaier, and Eugene S. Polzik, Room-temperature single-photon source with near-millisecond built-in memory, Nat. Commun. **12**, 3699 (2021).
[21] Yunfei Wang, Jianfeng Li, Shanchao Zhang, Keyu Su, Yiru Zhou, Kaiyu Liao, Shengwang Du, Hui Yan, and Shi-Liang Zhu, Efficient quantum memory for single-photon polarization qubits, Nat. Photonics **13**, 346 (2019).
[22] Mingtao Cao, Félix Hoffet, Shuwei Qiu, Alexandra S. Sheremet, and Julien Laurat, Efficient reversible entanglement transfer between light and quantum memories, Optica **7**, 1440 (2020).
[23] Gianni Buser, Roberto Mottola, Björn Cotting, Janik Wolters, and Philipp Treutlein, Single-photon storage in a ground-state vapor cell quantum memory, PRX Quantum **3**, 020349 (2022).
[24] D. Felinto, C. W. Chou, J. Laurat, E. W. Schomburg, H. de Riedmatten, and H. J. Kimble, Conditional control of the quantum states of remote atomic memories for quantum networking, Nat. Phys. **2**, 844 (2006).
[25] Zhen-Sheng Yuan, Yu-Ao Chen, Shuai Chen, Bo Zhao, Markus Koch, Thorsten Strassel, Yong Zhao, Gan-Jun Zhu, Jörg Schmiedmayer, and Jian-Wei Pan, Synchronized Independent Narrow-Band Single Photons and Efficient Generation of Photonic Entanglement, Phys. Rev. Lett. **98**, 180503 (2007).
[26] Yun-Fei Pu, Sheng Zhang, Yu-Kai Wu, Nan Jiang, Wei Chang, Chang Li, and Lu-Ming Duan, Experimental demonstration of memory-enhanced scaling for entanglement connection of quantum repeater segments, Nat. Photonics **15**, 374 (2021).
[27] Keyu Su, Yunfei Wang, Shanchao Zhang, Zhuoping Kong, Yi Zhong, Jianfeng Li, Hui Yan, and Shi-Liang Zhu, Synchronization and phase shaping of single photons with high-efficiency quantum memory, Chin. Phys. Lett. **38**, 094202 (2021).
[28] Chao-Ni Zhang, Hang Li, Jian-Peng Dou, Feng Lu, Hong-Zhe Yang, Xiao-Ling Pang, and Xian-Min Jin, Hong-Ou-Mandel interference linking independent room-temperature quantum memories, Photonics Res. **10**, 2388 (2022).
[29] See Supplemental Material at http://link.aps.org/supplemental/10.1103/PhysRevLett.131.033601 for a comparison of different photon synchronization experiments, more experimental details, and details of the theoretical models, which includes Refs. [30–33].
[30] Taek Jeong, Yoon-Seok Lee, Jiho Park, Heonoh Kim, and Han Seb Moon, Quantum interference between autonomous single-photon sources from doppler-broadened atomic ensembles, Optica **4**, 1167 (2017).
[31] Martin J. Stevens, Chapter 2—photon statistics, measurements, and measurements tools, in *Single-Photon Generation and Detection*, edited by Alan Migdall, Sergey V. Polyakov, Jingyun Fan, and Joshua C. Bienfang, Volume 45 of Experimental Methods in the Physical Sciences (Academic Press, New York, 2013), pp. 25–68.
[32] P. Grangier, G. Roger, and A. Aspect, Experimental evidence for a photon anticorrelation effect on a beam splitter: A new light on single-photon interferences, Europhys. Lett. **1**, 173 (1986).
[33] Jinxian Guo, Xiaotian Feng, Peiyu Yang, Zhifei Yu, L. Q. Chen, Chun-Hua Yuan, and Weiping Zhang, High-performance raman quantum memory with optimal control in room temperature atoms, Nat. Commun. **10**, 148 (2019).
[34] Jun-ichi Yoshikawa, Kenzo Makino, Shintaro Kurata, Peter van Loock, and Akira Furusawa, Creation, Storage, and On-Demand Release of Optical Quantum States with a Negative Wigner Function, Phys. Rev. X **3**, 041028 (2013).
[35] Kenzo Makino, Yosuke Hashimoto, Jun ichi Yoshikawa, Hideaki Ohdan, Takeshi Toyama, Peter van Loock, and Akira Furusawa, Synchronization of optical photons for quantum information processing, Sci. Adv. **2**, e1501772 (2016).
[36] Xiao-Ling Pang, Ai-Lin Yang, Jian-Peng Dou, Hang Li, Chao-Ni Zhang, Eilon Poem, Dylan J. Saunders, Hao Tang, Joshua Nunn, Ian A. Walmsley, and Xian-Min Jin, A hybrid quantum memory-enabled network at room temperature, Sci. Adv. **6**, eaax1425 (2020).

[37] Evan Meyer-Scott, Nidhin Prasannan, Ish Dhand, Christof Eigner, Viktor Quiring, Sonja Barkhofen, Benjamin Brecht, Martin B. Plenio, and Christine Silberhorn, Scalable Generation of Multiphoton Entangled States by Active Feed-Forward and Multiplexing, Phys. Rev. Lett. **129**, 150501 (2022).

[38] Zhibo Hou, Jun-Feng Tang, Chang-Jiang Huang, Yun-Feng Huang, Guo-Yong Xiang, Chuan-Feng Li, and Guang-Can Guo, Entangled-State Time Multiplexing for Multiphoton Entanglement Generation, Phys. Rev. Appl. **19**, L011002 (2023).

[39] Yoon-Seok Lee, Sang Min Lee, Heonoh Kim, and Han Seb Moon, Highly bright photon-pair generation in doppler-broadened ladder-type atomic system, Opt. Express **24**, 28083 (2016).

[40] Omri Davidson, Ran Finkelstein, Eilon Poem, and Ofer Firstenberg, Bright multiplexed source of indistinguishable single photons with tunable GHz-bandwidth at room temperature, New J. Phys. **23**, 073050 (2021).

[41] Omri Davidson, Ohad Yogev, Eilon Poem, and Ofer Firstenberg, Bright, low-noise source of single photons at 780 nm with improved phase-matching in rubidium vapor, arXiv:2301.06049.

[42] Ran Finkelstein, Eilon Poem, Ohad Michel, Ohr Lahad, and Ofer Firstenberg, Fast, noise-free memory for photon synchronization at room temperature, Sci. Adv. **4**, eaap8598 (2018).

[43] Omri Davidson, Ohad Yogev, Eilon Poem, and Ofer Firstenberg, Fast, noise-free atomic optical memory with 35% end-to-end efficiency, Commun. Phys. **6** 131 (2023).

[44] K. T. Kaczmarek, P. M. Ledingham, B. Brecht, S. E. Thomas, G. S. Thekkadath, O. Lazo-Arjona, J. H. D. Munns, E. Poem, A. Feizpour, D. J. Saunders, J. Nunn, and I. A. Walmsley, High-speed noise-free optical quantum memory, Phys. Rev. A **97**, 042316 (2018).

[45] H. H. Jen, Positive-p phase-space-method simulation of superradiant emission from a cascade atomic ensemble, Phys. Rev. A **85**, 013835 (2012).

[46] Ran Finkelstein, Ohr Lahad, Itsik Cohen, Omri Davidson, Shai Kiriati, Eilon Poem, and Ofer Firstenberg, Continuous Protection of a Collective State from Inhomogeneous Dephasing, Phys. Rev. X **11**, 011008 (2021).

[47] C. K. Hong, Z. Y. Ou, and L. Mandel, Measurement of Subpicosecond Time Intervals between Two Photons by Interference, Phys. Rev. Lett. **59**, 2044 (1987).

[48] Alexey V. Gorshkov, Axel André, Michael Fleischhauer, Anders S. Sørensen, and Mikhail D. Lukin, Universal Approach to Optimal Photon Storage in Atomic Media, Phys. Rev. Lett. **98**, 123601 (2007).

[49] Alexey V. Gorshkov, Axel André, Mikhail D. Lukin, and Anders S. Sørensen, Photon storage in Λ-type optically dense atomic media. II. Free-space model, Phys. Rev. A **76**, 033805 (2007).